Journal of Power Sources 196 (2011) 8012–8018

Contents lists available at ScienceDirect

Journal of Power Sources

journal homepage: www.elsevier.com/locate/jpowsour

Thermal insulation of muscovite/glass ceramic foam for solid oxide fuel cell

Da-Wei Liaw, Chu-Yu Tsai, Wen-Cheng J. Wei*,[1]

Department of Materials Science and Engineering, National Taiwan University, Taipei 10617, Taiwan, ROC

ARTICLE INFO

Article history:
Received 29 March 2011
Received in revised form 6 May 2011
Accepted 12 May 2011
Available online 19 May 2011

Keywords:
Thermal conductivity
Foam
Muscovite
Glass
Permeability

ABSTRACT

A direct foaming method of dispersed suspensions containing muscovite particulates and a glass powder ($47BaO–21B_2O_3–27SiO_2–5Al_2O_3$, in mol%) is used to prepare porous ceramic structures. The sintered foams exhibit extremely low thermal conductivity and slight expansion during the thermal treatment at 1000 °C. Both the foam stability and its thermal conductivity are investigated by considering foaming agents, muscovite/glass ratios, solid contents, microwave drying, wetting behaviors, and foam consolidation. One of the muscovite/glass ceramic foam, thermally treated at 950 °C for 1 h, showed the lowest thermal conductivity of 0.18 $W m^{-1} K^{-1}$ at 800 °C among all of the prepared samples. Its gas permeability and compressive strength are 0.1×10^{-7} cm^2 and 440 kPa, respectively.

1. Introduction

Solid oxide fuel cells (SOFCs) are designed to operate at temperatures between 500 and 1000 °C, at which sufficient ionic conduction of oxygen ion and good fuel reforming can be achieved. However, the thermal radiation, which results in heat dissipation during the operation, is relatively significant at such temperatures. Hence, a good thermal insulation is regarded as one of the energy saving strategies for thermal management of SOFCs. Oxides are a better choice than metals and polymers as the insulating materials for SOFCs.

Conventional insulating materials are made either by sintering ceramic powder or by the assembly of ceramic fibers. The forming processes usually induce a serious problem of dimension shrinkage after sintering, and the dimensional control of conventional insulators is poor. Therefore, a thermal insulator without significant shrinkage produced by colloidal processes, where platy muscovite was mixed with glass powder, was implemented in this study. The thermal insulator consists of ceramic foams can be used to seal the gaps between the SOFC components that are operated in the range of 27–800 °C.

There are three forming processes reported in the literature, replicas, sacrificial templates, and direct foaming methods [1–3]. However, both the replica and sacrificial template methods require sacrificial materials which can be burnt out after an appropriate pyrolysis process to create ceramic struts. Also, the pyrolysis process normally needs long thermal treatment due to a slow heating rate. However, high heating rates easily induce cracks within the porous structure during the pyrolysis and the burn-out rate for removing the organic material is the critical factor [4,5]. Compared to these two methods, the direct foaming method has the potential to overcome the problems of cracking and shrinkage induced by the long-time thermal treatment to obtain a uniform foam structure.

Using the direct foaming method, the porosity in the ceramics is generated by physically blowing air into the ceramic suspension. The porosity and the pore size of the final porous products are controlled primarily by the composition and the solid to liquid ratio. Moreover, the stability of air bubbles in the ceramic solution is the other crucial issue and is usually dominated by the surface chemistry of the solid ceramic particles [1,6–8].

The heat transfer in a porous material is dominated by three mechanisms, phonon conduction (K_{phonon}), photon conduction (K_{poton}) and convection ($K_{convection}$). A summation of these three contributions is considered as the resultant thermal conductivity (K_e) of a porous material, as shown in Eq. (1) [9].

$$\kappa_e = \kappa_{phonon} + \kappa_{photon} + \kappa_{convection} \quad (1)$$

The phonon conduction and the convection in solid phase are a function of T^{-1} and T, respectively. Additionally, the photon conduction is proportional to the third power of the temperature (i.e., $\propto T^3$). Hence, the photon contribution is obviously greater than the combined effects of phonon conduction and convection at higher temperatures, especially in the 500–650 °C range for an intermediate temperature SOFC (IT-SOFC).

* Corresponding author. Tel.: +886 2 33661317; fax: +886 2 23634562.
E-mail address: wjwei@ntu.edu.tw (W.-C.J. Wei).
[1] Present address: Department of Materials Science and Engineering, National Taiwan University, No. 1, Sec. 4, Roosevelt Road, Taipei 10617, Taiwan, ROC.

0378-7753/$ – see front matter © 2011 Elsevier B.V. All rights reserved.
doi:10.1016/j.jpowsour.2011.05.027

Table 1
Summary of the properties of porous ceramic foams investigated in this study.

Sample	Solid loading (vol%)		D/σ (μm)	ρ (g cm^{-3})	P (%)	K (10^{-7} cm^2)	κ (W m^{-1} K^{-1})		
	Muscovite	Glass					25 °C	600 °C	800 °C
M1G1_stir	8.0	0.9	140/70	0.071	97.5	8.6	0.09	0.21	0.28
M1G2_stir	8.0	3.5	141/60	0.076	97.4	5.1	0.09	0.19	0.26
M1G3_stir	8.0	7.5	123/53	0.110	96.3	2.4	0.10	0.19	0.25
M3G1_stir	10.0	0.9	80/43	0.079	97.0	2.9	0.10	0.21	0.27
M3G2_stir	10.0	3.5	85/42	0.101	96.2	2.0	0.10	0.20	0.26
M3G3_stir	10.0	7.5	69/24	0.190	93.5	1.7	0.10	0.19	0.24
M1G1_shake	8.0	0.9	157/57	0.079	97.2	4.2	0.10	0.18	0.24
M1G2_shake	8.0	3.5	152/52	0.088	96.9	2.0	0.08	0.17	0.23
M1G3_shake	8.0	7.5	128/45	0.157	94.6	0.5	0.09	0.18	0.23
M3G1_shake	10.0	0.9	86/24	0.129	95.4	0.4	0.08	0.15	0.22
M3G2_shake	10.0	3.5	94/24	0.184	93.6	0.2	0.08	0.14	0.18
M3G3_shake	10.0	7.5	71/20	0.260	91.2	0.1	0.08	0.14	0.18
Porous Al_2O_3[a]	4.76 vol%, pH = 6, SDS surfactant		80	0.280	93.0	Not measured	0.10	0.20	0.27

D, average cell size; σ, standard deviation; P, porosity; K, permeability; κ, thermal conductivity.
[a] The properties of a porous alumina are reported according to Lo's work [20].

To produce light-weight and low-thermo-conductive ceramic foams, this study used a foaming and microwave-drying process without significant distortion or shrinkage. Because the crystalline structure of muscovite (a kind of platy minerals) with low symmetry has greater ability to impede the heat transfer by phonon and photon conduction [10], platy muscovite, which has a density as low as 2.76 g cm^{-3}, was selected as the skeleton for the novel thermal insulator in this study. The platy muscovite particulates were wetted using melted glass in porous conditions during the thermal treatment, forming a composite to scatter the photons. The properties of porous ceramics, such as the porosity, gas cell sizes, and gas permeability, were measured and discussed with respect to thermal conductivity and compressive strength.

2. Experimental procedure

The fabrication procedures include the preparation of dispersive slurries, direct foaming using high-speed stirring, microwave drying, organic burnouts, and consolidation. After fabrication, the essential analyses, including porosity, permeability, thermal-mechanical analyses (TMA), thermal conductivity, compressive strength and scanning electron microscopy (SEM) observation, were then conducted.

Two kinds of ceramic powders, G1A5 glass ($46.55BaO–27.86SiO_2–20.46B_2O_3–5.12Al_2O_3$ in mol%) and muscovite ($KAl_2(AlSi_3O_{10})OH_2$), were used in this study. The formulation and melting properties of the G1A5 glass were developed and investigated by Chang et al. [11]. The G1A5 glass powder was produced by the Exojet Technology Corporation (Shin-Chu, Taiwan). The morphologies of these two powders are shown in Fig. 1.

Several surfactants were tried in this study. Only a cationic dispersant, (lauryl dimethybenzyl ammonium chloride, $C_{21}H_{38}ClN$, abbreviated as "CDB", with 50% water content, Sino-Japan Chemical, Taiwan) was found to be suitable for preparing muscovite/G1A5 porous ceramics.

Methods similar to those described in the literature [12–16] were adopted in the present study to ensure long-term stability of muscovite/glass foams using the CDB chemical in aqueous suspension. In addition, the planetary ball-mill was used to treat the formulated samples shown in Table 1 for 18 h to obtain various ceramic foams. After the ball milling, extra stirring (with the "-R" after sample notation) or shaking ("-K") for 1 min was also used to increase the stability of the foams. The produced foams can be used to seal a gap less than 2 mm resulting in extremely low gas leakage after drying [10].

As-foamed samples were dried in a microwave oven (Multiwave 3000, Anton Paar Gmbh, Graz, Austria). For a wet foam sample containing 40 ml of water as an example, the microwave process was operated at a rate of 5 W min^{-1} from 0 W to 20 W and then held 90 min at 20 W. Afterward, the sample was continually heated by microwaves with an increasing power at a rate of 1 W min^{-1} from 20 W to 30 W, and then held for 90 min at 30 W.

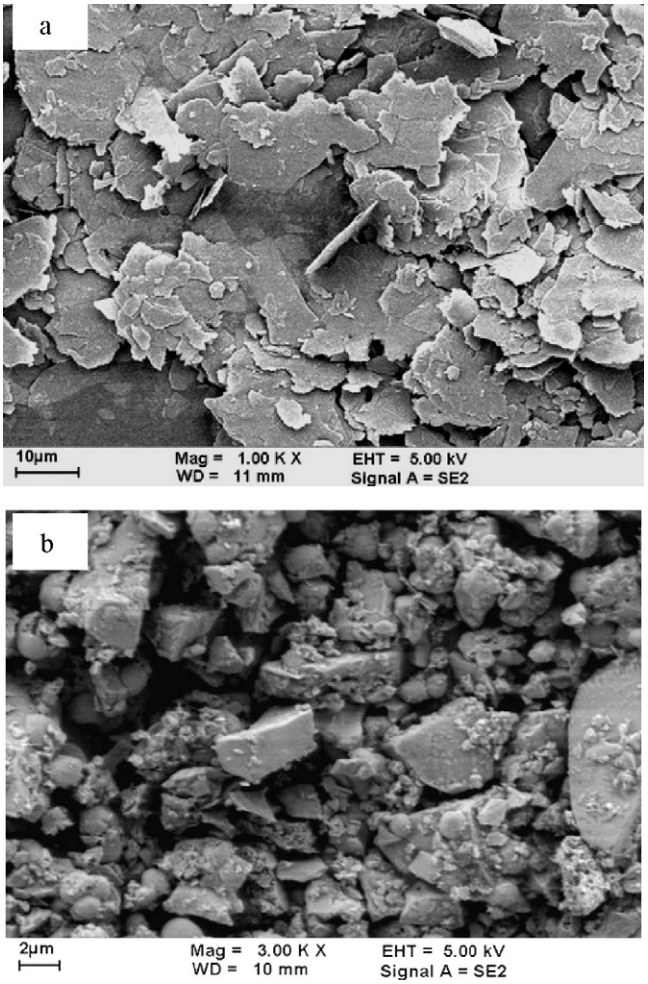

Fig. 1. SEM micrographs revealing the morphologies of (a) muscovite and (b) G1A5 powders.

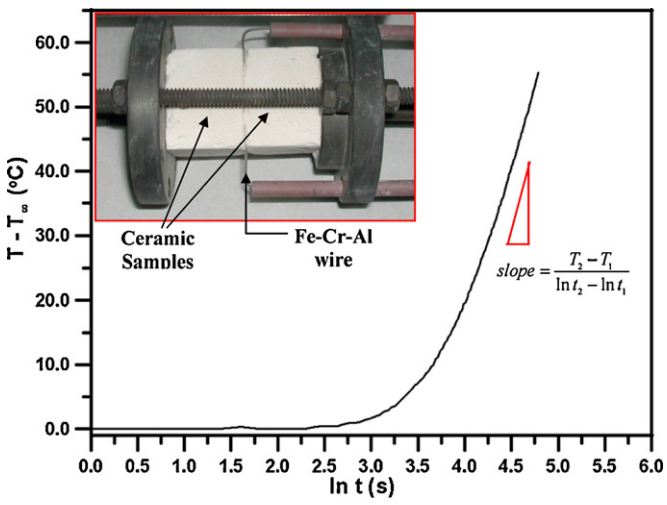

Fig. 2. Heating time t in log scale plotted against the temperature difference $(T - T_\infty)$ with an insert picture illustrating the arrangement of ceramic samples and the Fe–Cr–Al wire between the steel fixtures.

One of the potential advantages of developing such insulated foams were realized [10] that the melted glass can bond muscovite particulates strongly. The glass particles can be melted completely at 950 °C in 1 h after prior organic burnout at 600 °C for 1 h. Another great advantage of using the melted glass to wet the muscovite particles is to prevent the volume shrinkage of the ceramic foam.

The porosity P of the investigated foam was calculated using the following equation:

$$P = \left(1 - \frac{\rho_s}{\rho_{th}}\right) \times 100\% \tag{2}$$

where ρ_s is the apparent density of the sample and ρ_{th} is the theoretical density of the solid mixture, which can be calculated using the following equation:

$$\rho_{th} = \frac{100}{(W_{mica}/\rho_{mica} + W_{glass}/\rho_{glass})} \tag{3}$$

where W_{mus} and W_{G1A5} are, respectively, the mass percentages of the muscovite and G1A5 glass as the solid phase of the sample, and ρ_{mus} and ρ_{glass} are the theoretical densities of muscovite and G1A5 glass, respectively.

The average grain size was measured using scanning electron microscopy (SEM) with the line-intercept function. The measured values were multiplied by 1.56 to calibrate the grain size [17].

The permeability analysis was performed by giving a specific gas flow rate Q and then measuring the pressure difference ΔP across the porous ceramic sample. The permeability K can then be calculated according to Darcy's law as shown below [18].

$$K = \frac{Q}{A}\frac{L}{\Delta P}\mu, \tag{4}$$

where A is the sectional area of the sample, L is the sample length, and μ is the dynamic viscosity of the air ($\mu_{\text{air, 23°C}} = 1.83 \times 10^{-4}$ dyne scm^{-2}). The air, instead of H_2, was used to measure the permeability because oxygen molecules are the oxidant used for SOFC with ZrO_2-based electrolyte.

The thermal conductivity was measured using a hot-wire method and the instrument is shown in Fig. 2. Fe–Cr–Al wire (0.0217 Ω cm^{-1}) was used as a heating source by embedding the wire between two identical ceramic samples. A thermocouple was inserted into the ceramic sample and kept a distance of 0.80 cm away from the Fe–Cr–Al wire. A constant current of 10 A was provided to the Fe–Cr–Al wire and the temperature variation was detected using a thermocouple. By plotting the temperature increment $(T - T_\infty$, where T_∞ is the ambient temperature) against $\ln t$ and measuring the slope (S) of the straight section of the line, as illustrated in Fig. 2, the thermal conductivity of the sample is calculated according to Eq. (5).

$$\kappa = A\frac{Q}{4\pi L}\frac{\ln t_2 - \ln t_1}{T_2 - T_1} = A\frac{Q}{4\pi L}\frac{1}{S} \tag{5}$$

where A is calibration factor, T_1 and T_2 are the temperature increment detected at time t_1 and t_2, respectively, by the thermocouple, Q is the input heat, L is the sample length and t is the heating time.

The calibration was carried out by measuring a standard sample provided by China Steel Corporation and the reported thermal conductivity was 0.295 W m^{-1} K^{-1} at 298 K and 0.35 W m^{-1} K^{-1} at 773 K. The calibration factors (A) at 25 °C and 500 °C were 1.76 and 1.97, respectively. The calibration factors at other temperatures were calculated using liner interpolation.

The relation between the thermal conductivity and the microstructure was characterized. The properties of porous ceramics, such as the porosity, cell sizes, gas permeability were measured using SEM micrographs and the compressive strength was measured using a compressive testing machine (810 MTS Co., USA).

3. Results and discussion

3.1. Stabilization of ceramic foams

The stability of ceramic foams is determined by the microstructure of the porous ceramics. The morphologies of the muscovite and G1A5 in the ceramic foam were observed by SEM and were shown in Fig. 1. The muscovite particulates exhibit a platy shape, while the G1A5 particulates exhibit a granular shape. As the platy particulates cover the bubble surfaces and form an outside crust, more stable bubbles accumulate through the interlocking of muscovite particulates. The stability of the foam is determined by the solid muscovite load in the ceramic slurry. Because bubble coalescence is significantly constrained by platy particulates, the cell size and the cell size distribution are fairly stable as listed in Table 1. The glass particulates, however, do not induce a remarkable interlocking mechanism as muscovite particulates do. Accordingly, the cell size and the cell size distribution of the porous ceramic are primarily affected by the muscovite rather than the G1A5 glass.

3.2. Porosity and permeability

According to Table 1, the porosity and permeability decrease with the increase in the solid loading of the glass and muscovite powders. For example, M3G1_K and M3G3_K have the same muscovite content but the different G1A5 glass content from 0.9 vol% up to 7.5 vol%, and the porosity and permeability are decreased from 95.4% to 91.2% and from 0.4×10^{-7} cm^2 to 0.1×10^{-7} cm^2, respectively. In contrast, M1G3_K and M3G3_K have the same G1A5 glass content but the different muscovite content from 8.0 vol% to 10.0 vol%, and the porosity and permeability are decreased from 94.6% to 91.2% and from 0.5×10^{-7} cm^2 to 0.1×10^{-7} cm^2. Hence, both the 2 vol% increase in muscovite and the 6.6 vol% increase in G1A5 glass have approximately the same influence on the permeability. Also, the samples prepared by shaking have a lower permeability than those prepared by stirring, as listed in Table 1.

The permeability of the forms is mainly controlled by the porosity of the cell walls, which is greatly dependent on the relative content of the glass to muscovite. The sintered M1G1_R ceramic foam with 8 mol% of muscovite and small amount (0.9 vol%) of glass showed less sintering (more porosity) than those with higher glass content (7.5 vol%). High glass content was melted between platy muscovite particulates and sealed the gaps on cell walls after sin-

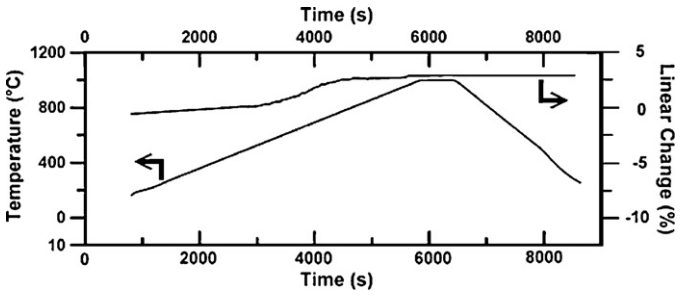

Fig. 3. TMA analysis of the die-pressed muscovite disk. The muscovite specimen was de-hydrated at 600 °C for 2 h before the TMA test.

tering. The SEM image in Fig. 10 is one example to depict the state of closed porosity of the cell wall.

Comparing the porosity of the samples to that of porous alumina in Table 1, all of the samples except M3G3_shake have porosities in a range of 93.5–97.5%, which is larger than that of porous alumina with 93.0% porosity.

Fig. 3 shows the TMA analysis of muscovite. No obvious sintering shrinkage occurred even at temperatures as high as 1000 °C and, specifically, the linear expansion is ~ 2.5%. The TMA analysis of muscovite mixed with ~ 40 vol% glass was also tested and shown in Fig. 4. The 2% linear shrinkage which occurs at temperatures of about 900 °C results from the softening and melting of G1A5 glass. The muscovite/glass has about 10% expansion after sintering at 950 °C for 1 h. If the solid load is reduced to less than 10 vol% and the porosity increases to larger than 90%, a slight expansion of the porous foam should be obtained after the consolidation process at 950 °C for 1 h [10].

The melting temperature of G1A5 glass is approximately 880 °C [11]. It starts wetting the muscovite particle surface as the temperature increases, as shown in Fig. 5. To ensure that all G1A5 glass particles melt between the muscovite particulates, the temperature of consolidation process is set at 950 °C. The wetting behavior of G1A5 glass plays an important role in bonding the muscovite particulates together to provide the required strength (e.g. compressive strength) for forming a porous ceramic foam structure.

3.3. Compressive strength

Compressive strength is an important property for thermal insulators. Accordingly, the strengths of three M3 samples were

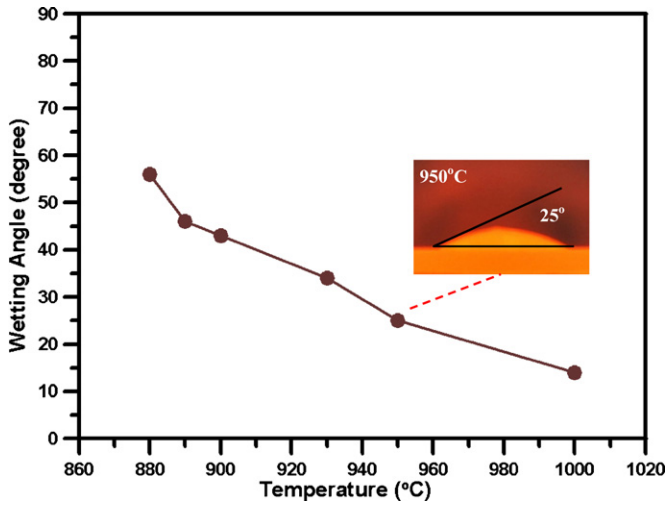

Fig. 5. Wetting behavior of the G1A5 glass pellet on the muscovite substrate at the temperature between 880 °C and 1000 °C. Each temperature was hold for 5 min before the measurement.

investigated in this study. As shown in Fig. 6, the stress–strain curves of the porous ceramics show a graceful failure mode. The compressive strength increases from 114 to 440 kPa with both the increase in G1A5 glass content from 0.9 vol% to 7.5 vol% and the decrease in porosity from 95.4% to 91.2%. The strength of the porous ceramics is provided primarily by the glass phases, which have melted between the platy muscovite particulates and appropriately bonding to the particulates. Both the increase in density and the reduction in porosity result in denser microstructures and thus increase the compressive strength.

A similar result for the dependence of the compressive strength of porous ceramics on porosities has been reported in the literature [19], as shown in Fig. 7. The compressive strengths of the particle-stabilized porous alumina are less than 10 MPa when porosities are between 86.0% and 88.5%. The compressive strengths of surfactant-stabilized alumina foams are between 3.5 MPa and 90 kPa with porosities between 85.0% and 96.0%. Moreover, the compressive strengths of the investigated samples, M3G1_K, M3G2_K and M3G3_K with porosities ranging from 95.4% to 91.2%, increased from 114 kPa to 440 kPa. These muscovite/glass samples have the

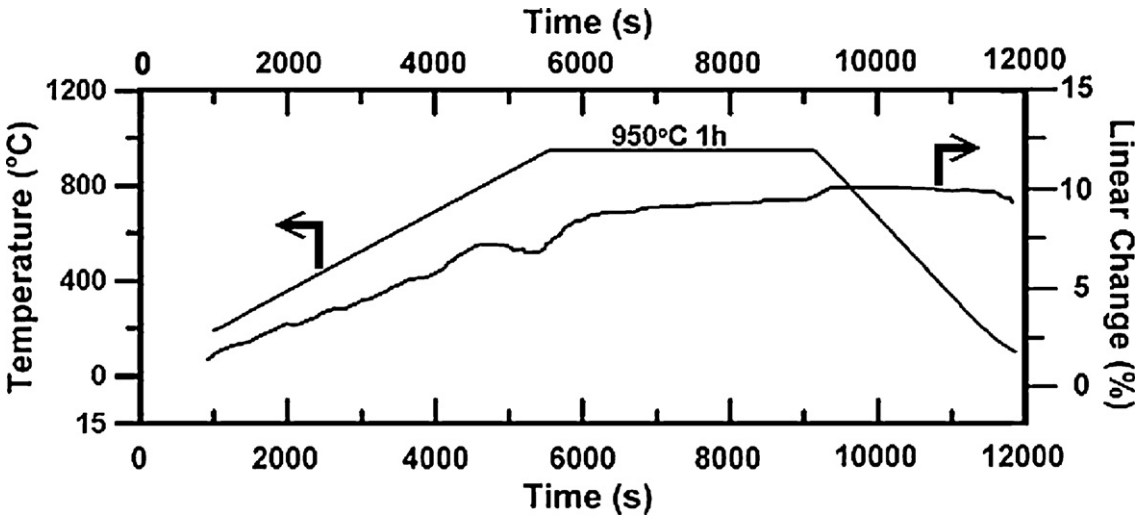

Fig. 4. TMA analysis of the die-pressed muscovite/glass disk which contains 57.1 vol% of muscovite and 42.9 vol% of G1A5 glass shows shrinkage occurred at about 900 °C, which resulted from the melting of the G1A5 glass. The specimen was de-hydrated at 600 °C for 2 h before the TMA test.

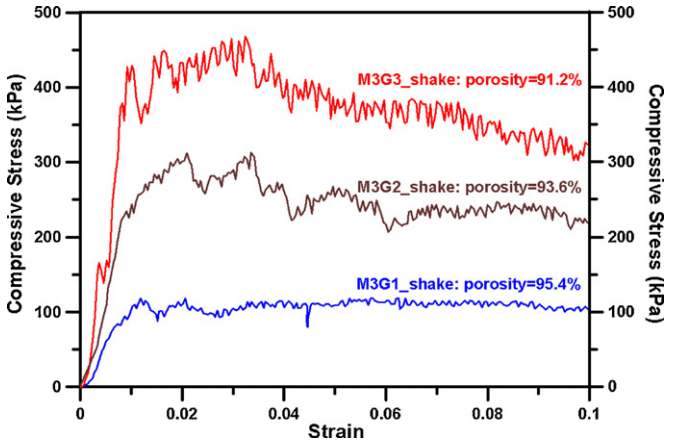

Fig. 6. Stress–strain curves of investigated porous ceramics, showing a gradual failure mode.

similar compressive strengths as compared to the surfactant stabilized alumina, for which the strength is approximately 90–700 kPa.

3.4. Thermal conductivity

The last three columns of Table 1 show the thermal conductivities of muscovite/glass and Al_2O_3 foams. The conductivities are in the 0.08–0.10 $W\,m^{-1}\,K^{-1}$ range at room temperature and increase to the range of 0.18–0.28 $W\,m^{-1}\,K^{-1}$ at 800 °C. The conductivity of the foams is also attributed to the phonon and convection conduction in the air, which depends on the 1st power of the temperature (T) rather than 3rd power of the temperature (T^3). In contrast, the photon conduction could be the dominant mechanism of the heat transfer if the porous ceramics are used at elevated temperatures. The function of the photon conduction is dominated primarily by the 3rd power of the temperature (T^3), as shown in Eq. (6).

$$\kappa_{photon} = A + BT^3 \tag{6}$$

Accordingly, the calibrated thermal conductivities of four foams after excluding the influence of the air are plotted in Fig. 8. The fitting curves using Eq. (6) show quite well fitting except M1G3_K, which shows a linear relationship to the temperatures below 400 °C.

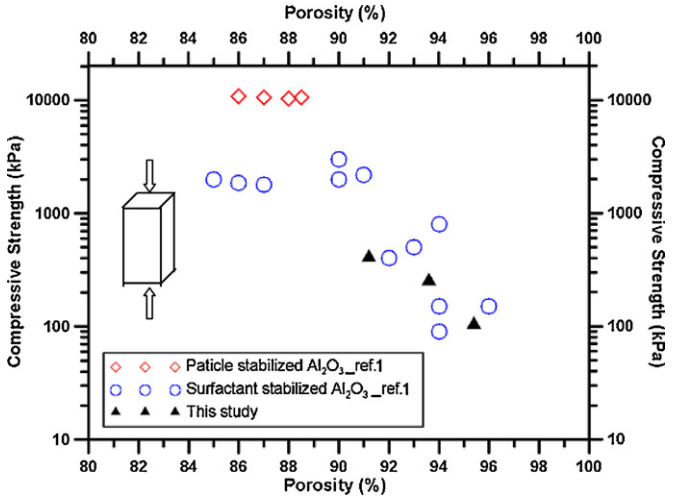

Fig. 7. Comparison of the compressive strength of investigated samples with that reported in literature [1,19]. Specimens for the compressive strength in this study were produced to have a square cross section and an aspect ratio of 2.0 (11 mm × 11 mm × 22 mm).

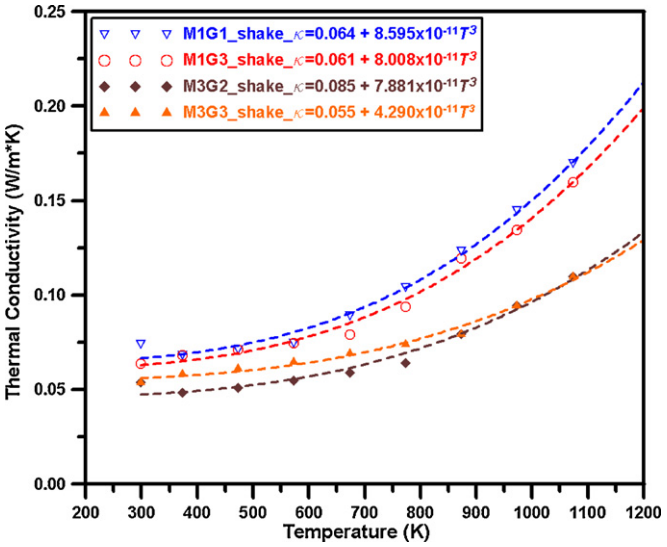

Fig. 8. Calibrated thermal conductivity of sample M1G1_K, M1G3_K, M3G2_K and M3G3_K plotted against testing temperatures after deducting the thermal conductivity contribution of the air.

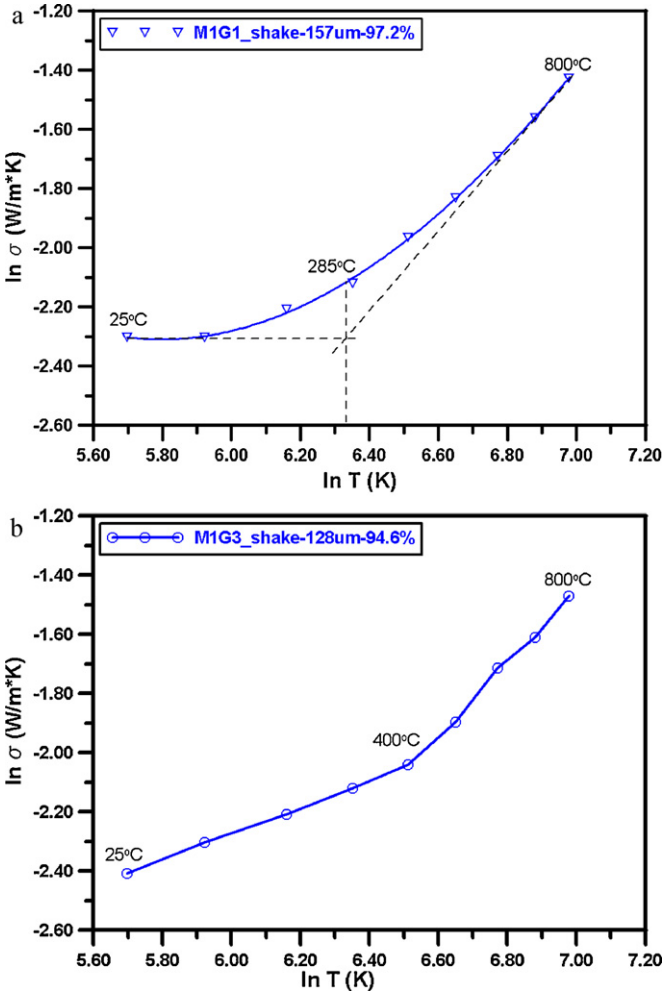

Fig. 9. Thermal conductivity analysis of two samples (a) M1G1_K and (b) M1G3_K plotted against the temperature in a log scale. The critical temperatures at which the photon conduction becomes significant are at ~285 °C and ~400 °C, respectively.

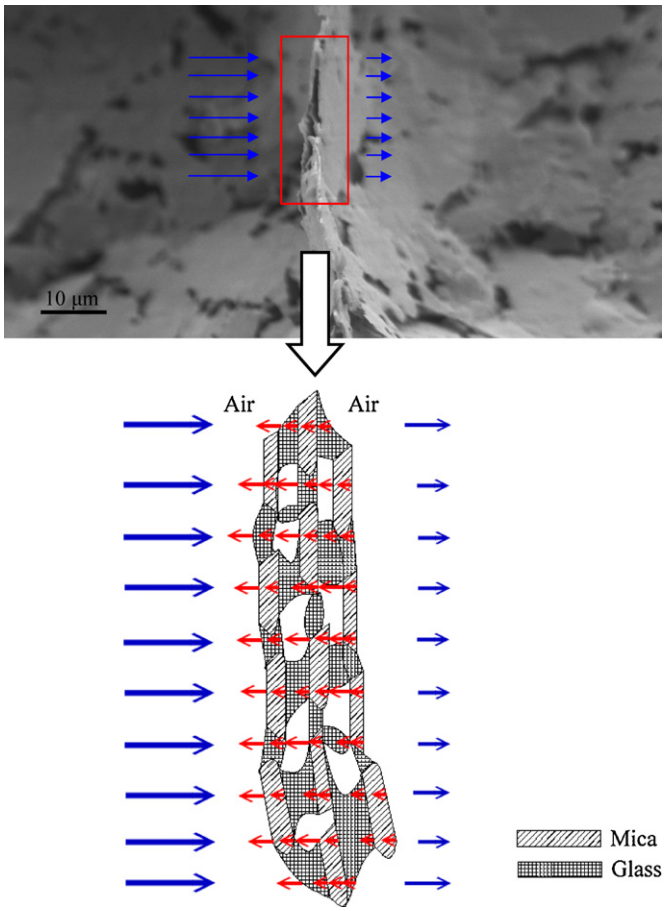

Fig. 10. SEM picture of muscovite/glass cell walls and a schematic illustration of the incident radiation (filled arrows) traveling through the multilayer cell wall structure. The reflection occurs at each interface, and each of reflection causes a reduction in the intensity of the incident radiation.

A more detailed analysis of the contribution from photons or phonons was conducted so to differentiate the contribution from different mechanisms. The critical temperature is defined by the transformation from the 1st power of the temperature dependence (T) to the 3rd power of the temperature dependence (T^3), as shown in Fig. 9. Both the thermal conductivity and the temperature in Fig. 9 are plotted based on the nature logarithm. The thermal conductivity increases slightly at low temperatures and significantly at high temperatures. At temperatures below the critical temperature, the increase in thermal conductivity results mostly from the increase in thermal conductivity of the air. The phonon conduction contributions from muscovite and glass are insignificant due to very low solid contents.

As shown in Fig. 9(a), the critical temperature is approximately at 285 °C when the average cell size is 157 μm. It shifts to 400 °C when the average cell size decreases to 128 μm, as shown in Fig. 9(b). A smaller average cell size leads to the enhancements of multilayer-scattering and reflection due to more interfaces generated. Therefore, the critical temperature tends to shift toward the high temperature with decreasing average cell size. In other words, more multilayer structures constructed by muscovite/glass cause more light scattering. When the incident radiation propagates through the cell walls, as shown in Fig. 10, the photon reflection occurs at the interfaces between muscovite and glass due to the different reflection indices. Each reflection causes a reduction in the flux of the transmitted photons, thus reducing photon conduction.

The conductivity properties of the investigated porous ceramic samples are listed in Table 1. The properties of one porous alumina sample, which had the best insulation property by Lo's report [20], are also listed at the bottom of the table as a reference. It is obvious that the lowest thermal conductivities, 0.08 W m^{-1} K^{-1}, 0.14 W m^{-1} K^{-1}, and 0.18 W m^{-1} K^{-1} at 25 °C, 600 °C, and 800 °C from different samples, were all lower than those from the porous alumina, which are 0.10 W m^{-1} K^{-1}, 0.20 W m^{-1} K^{-1}, and 0.27 W m^{-1} K^{-1} at 25 °C, 600 °C, and 800 °C, respectively. When the temperature increases from room temperature to the critical temperature, the thermal conduction by air was the dominant heat transfer mechanism. As the temperature became higher than the critical temperature, the photon conduction dominates the mechanism of heat transfer mechanism. Moreover, the effects of the pore-scattering and multilayer-reflection increased as the cell size was reduced.

4. Conclusions

This study produced light weight, low thermal conductivity, and slightly expanded porous ceramic foams consisting of muscovite and glass phases. The variations of the porosity and average cell sizes of the foams are mainly controlled by processing conditions, especially, solid content of the slurries and the amount of the platy muscovite.

The porosity of all prepared samples was between 91.2% and 97.5%, and the average cell size was between 69 μm and 157 μm. The permeability of all investigated samples was between 0.1×10^{-7} cm^2 and 8.6×10^{-7} cm^2, and decreased with the increase of the glass in the solid content. The glass content had more significant influences on the permeability than the other factors, e.g. muscovite content.

The lowest thermal conductivities of the foams obtained in this study were 0.08 W m^{-1} K^{-1} and 0.18 W m^{-1} K^{-1} at 25 °C and 800 °C, respectively, which were better than those of alumina foams in the same temperature range. The critical temperature that the control mechanism of thermal conductivity changed to photon conduction was ~285 °C when the average cell size of the sample was 157 μm. The critical temperature shifted to ~400 °C when the average cell size decreased to 71 μm. The photon conduction can be reduced by decreasing the cell size and porosity. Smaller cell sizes and lower porosity lead to an enhancement of the photon scattering and multilayer-reflection.

The compressive strengths of the foams were in the same range as the stabilized alumina foams reported in the literature, which were in the range of 90–700 kPa. Among all samples, the highest compressive strength was 440 kPa with the porosity of 91.2%.

Acknowledgements

The authors like to acknowledge the funding given by National Science Council in Taiwan (NSC99-2221-E-002-133-MY2) and helpful discussion by Professor C.H. Hsueh.

References

[1] U.T. Gonzenbach, A.R. Studart, E. Tervoort, L.J. Gauckler, Angew. Chem., Int. Ed. 45 (2006) 3526–3530.
[2] H.A. Wege, S. Kim, V.N. Paunov, Q. Zhong, O.D. Velev, Langmuir 24 (2008) 9245–9253.
[3] P. Colombo, Philos. Trans. R. Soc., A 364 (2006) 109–124.
[4] J. Saggio-Woyansky, C.E. Scott, W.P. Minnear, Am. Ceram. Soc. Bull. 71 (11) (1992) 1674–1682.
[5] O. Lyckfeldt, J.M.F. Ferreira, J. Eur. Ceram. Soc. 18 (2) (1998) 131–140.
[6] Z.P. Du, M.P. Bilbao-Montoya, B.P. Binks, E. Dickinson, R. Ettelaie, B.S. Murray, Langmuir 19 (8) (2003) 3106–3108.
[7] E. Dickinson, R. Ettelaie, T. Kostakis, B.S. Murray, Langmuir 20 (20) (2004) 8517–8525.
[8] B.P. Binks, T.S. Horozov, Angew. Chem., Int. Ed. 44 (24) (2005) 3722–3725.

[9] W.D. Kingery, H.K. Bowen, D.R. Uhlmann, Introduction to Ceramics, 2nd ed., John Wiley and Sons, USA, 1976.
[10] W.C.J. Wei, C.Y. Tsai, "Porous ceramic composite and manufacturing method thereof," Chinese patent application no. 099118809, files on June 9th, 2010.
[11] C.Y.S. Chang, W.C.J. Wei, C.H. Hsueh, J. Non-Cryst. Solid 357 (2011) 1414–1419.
[12] Y.W. Kim, C.B. Park, Compos. Sci. Technol. 63 (16) (2003) 2371–2377.
[13] P. Colombo, M. Modesti, J. Am. Ceram. Soc. 82 (3) (1999) 573–578.
[14] T. Takahashi, H. Munstedt, P. Colombo, M. Modesti, J. Mater. Sci. 36 (7) (2001) 1627–1639.
[15] G.S. Grader, G.E. Shter, Y. de Hazan, J. Mater. Res. 14 (4) (1998) 1485–1494.
[16] A.R. Studart, U.T. Gonzenbach, E. Tervoort, L.J. Gauckler, J. Am. Ceram. Soc. 89 (6) (2006) 1771–1789.
[17] M.I. Mendelson, J. Am. Ceram. Soc. 52 (1969) 443.
[18] A. Nabovati, E.W. Llewellin, A.C.M. Sousa, Composites: Part A 40 (2009) 860–869.
[19] U.T. Gonzenbach, A.R. Studart, E. Tervoort, L.J. Gauckler, J. Am. Ceram. Soc. 90 (1) (2007) 16–22.
[20] Y.W. Lo, W.C.J. Wei, C.H. Hsueh, Mat. Chem. Phy. (2011), doi:10.1016/j/matchemphys/2011/04.023.